Available online at www.sciencedirect.com

ScienceDirect

Ceramics International 40 (2014) 25–30

CERAMICS INTERNATIONAL

www.elsevier.com/locate/ceramint

Cerium carbonate hydroxide and ceria micro/nanostructures: Synthesis, characterization and electrochemical properties of $CeCO_3OH$

Fatma Hrizi, Hassouna Dhaouadi*, Fathi Touati

Laboratoire des Matériaux Utiles, INRAP, Technopôle Sidi-Thabet, Tunis 2020,Tunisie

Received 5 March 2013; received in revised form 26 April 2013; accepted 27 May 2013
Available online 31 May 2013

Abstract

Cerium hydroxide carbonate ($CeCO_3OH$) nano and microcrystals were synthesized by the hydrothermal method at 180 °C using cerium nitrate ($Ce(NO_3)_3 \cdot 6H_2O$) as the cerium source, urea as both an alkaline and carbonate source with cetyltrimetylammonium bromide (CTAB) as the directing agent. By varying many of the experimental parameters such as the molar ratio CTAB/$Ce(NO_3)_3 \cdot 6H_2O$ [CTAB/Ce], cerium hydroxide carbonate nanomaterials with different morphologies were obtained. However, cerium oxide (CeO_2) micro/nanostructure is obtained through the thermal decomposition of $CeCO_3OH$ at 300 °C for 1 h. X-ray powder diffraction (XRD), scanning electron microscopy (SEM) and thermal analyses (TG-DTA) were the techniques used to study the resulting products. The $CeCO_3OH$ microstructure exhibits an excellent electrochemical reversibility, which is an important feature with many applications such as in lithium ion batteries.
© 2013 Published by Elsevier Ltd and Techna Group S.r.l.

Keywords: B. X-ray methods; D. CeO_2; E. Electrodes

1. Introduction

Cerium oxides and their derivative compounds have received much attention due to their novel electronic and optical properties, and to their chemical characteristics arising from the 4f electrons from the cerium element [1]. Cerium oxide (CeO_2) nanocrystals are an important material because of their applications as an oxygen ion conductor in solid oxide fuel cells [2] and oxygen monitors [3] but also as a catalytic support of automotive exhaust systems due to their high oxygen conductivity [4]. In recent years, ceria with different morphologies and microstructures has been synthesized, including nanoparticles [5], nanowires [6], nanofibers [7], nanotubes [8], nanorods [9], nanocubes [10], solid spheres [11] and hollow spheres [12]. Furthermore, the synthesis of $CeCO_3OH$ has become representative of the cerium compound because, not only does it provide unique optical properties related to its different phase structures and morphologies, but also becomes the template precursor for synthesizing ceria with different morphologies through the thermal decomposition of $CeCO_3OH$ [13].

Shape-controlled ceria and cerium carbonate hydroxide with different morphologies have been prepared using various methods such as homogeneous precipitation, the hydrothermal method, sol–gel, microemulsion or reverse micelles and the microwave-hydrothermal method [14]. Among these preparation methods, the hydrothermal one is regarded as an effective process due to its low reaction temperature, because it is environmentally friendly, economic, and easy to be implemented [15].

Microstructure and photoluminescence studies have already been published on CeO_2 and its derivates [16–18]. Few researchers are devoted to the investigation of the electrochemical properties of CeO_2 [19,20]. Due to the direct and fast transformation of Ce(III) and Ce(IV), CeO_2 is believed to be a good candidate as an anode material for lithium ion batteries. However, there are still no reports on the electrochemical properties of the $CeCO_3OH$ nanomaterial. In this work, an

*Corresponding author. Tel.: +21 671 537666; fax: +21 671 537688.
E-mail address: dhaouadihassouna@yahoo.fr (H. Dhaouadi).

0272-8842/$ - see front matter © 2013 Published by Elsevier Ltd and Techna Group S.r.l.
http://dx.doi.org/10.1016/j.ceramint.2013.05.098

attempt has been made to study the electrochemical performance of $CeCO_3OH$ for its use as an electrode for lithium ion batteries.

Here, we report the synthesis and the characterization of cerium carbonate hydroxide nanocrystalline using the hydrothermal method in the presence of CTAB as the structure-directing template. Ceria micro/nanostructures were prepared by the thermal conversion of $CeCO_3OH$ in air at 300 °C. A set of experiments was carried out to study the influence of the [CTAB/Ce] molar ratio on the morphology and size of cerium carbonate hydroxide nanomaterials. The electrochemical properties of the $CeCO_3OH$ were also studied.

2. Experimental

2.1. Hydrothermal synthesis

The synthesis was carried out according to the following procedure: 0.27 mmol of $Ce(NO_3)_3 \cdot 6H_2O$ and a stochiometric amount of carbamide ($CO(NH_2)_2$) were placed in distilled water to form a clear solution, which was stirred strongly at room temperature for about 0.5 h. A given amount of CTAB was then added under magnetic stirring at room temperature for about 0.5 h. The clear solution obtained was transferred to a Teflon-lined stainless steel autoclave, which was sealed and maintained at 180 °C for 3 h, and then naturally cooled to room temperature. The resulting white precipitate was collected by filtration, washed three times with distilled water and then dried in air at 80 °C. The as-synthesized $CeCO_3OH$ was calcined in air at 300 °C for 1 h to produce yellow CeO_2.

In order to control the morphology and the particle size of the $CeCO_3OH$ products many experiments were performed varying the molar ratios of [CTAB/Ce] each time to: 1/1, 1/2 and 2/1.

2.2. Characterization

X-ray powder diffraction data (XRD) was obtained on an X'Pert Pro Panalytical diffractometer with CuK radiation (λ=1.54056 Å) and graphite monochromator. The texture of the samples prepared was examined using a scanning electron microscope (SEM) Quanta 200 (FEI). Thermal analyses (TG-DTA) were performed using a Setaram setsys 1750 at a heating rate of 5 °C/min^{-1} from 25 °C to 700 °C.

For electrochemical measurements the electrode used was prepared as follows: an aqueous suspension of 3 mg/mL of Ce$(CO_3)(OH)$ microstructures was prepared and 100 µL of this suspension were dropped into an ITO coated glass plate to cover a 1 cm^2 surface area. The electroactivity of the $CeCO_3OH$ microstructures was measured using the same cell containing 0.1 M lithium perchlorate ($LiClO_4$) as the support electrolyte in an aprotic solution of propylene carbonate (PC). Cyclic voltammetry (CV) measurements were carried out at a sweep rate of 5 mV/s over the range [−1.0 to +1.5 V/SCE]. Electrochemical measurements were carried out using one compartment cell and Biologic SP150 potentiostat/galvanostat apparatus.

3. Results and discussion

3.1. X-ray diffraction

Typical XRD patterns of the as-prepared sample are shown in Fig. 1a. All the diffraction peaks characterize the orthorhombic crystalline phase of $CeCO_3OH$ with lattice parameters a=5.015 Å, b=8.565 Å and c=7.337 Å (JCPDS 41-0013). No peaks of any other phases or impurities were detected, indicating the high purity of the as-obtained $CeCO_3OH$ phase. Moreover, the relative intensity of the reflection of (012) to that of (110) peaks is much stronger than that of bulk materials in the JCPDS card (Fig. 1b), indicating the presence of preferred orientation.

3.2. Scanning electron microscopes

In order to study the effect of the molar ratio [CTAB/Ce] on the product structure and morphology, the experiments were carried out at 180 °C for 3 h by using different molar ratios of [CTAB/Ce]. Fig. 2 shows SEM images of the $CeCO_3OH$

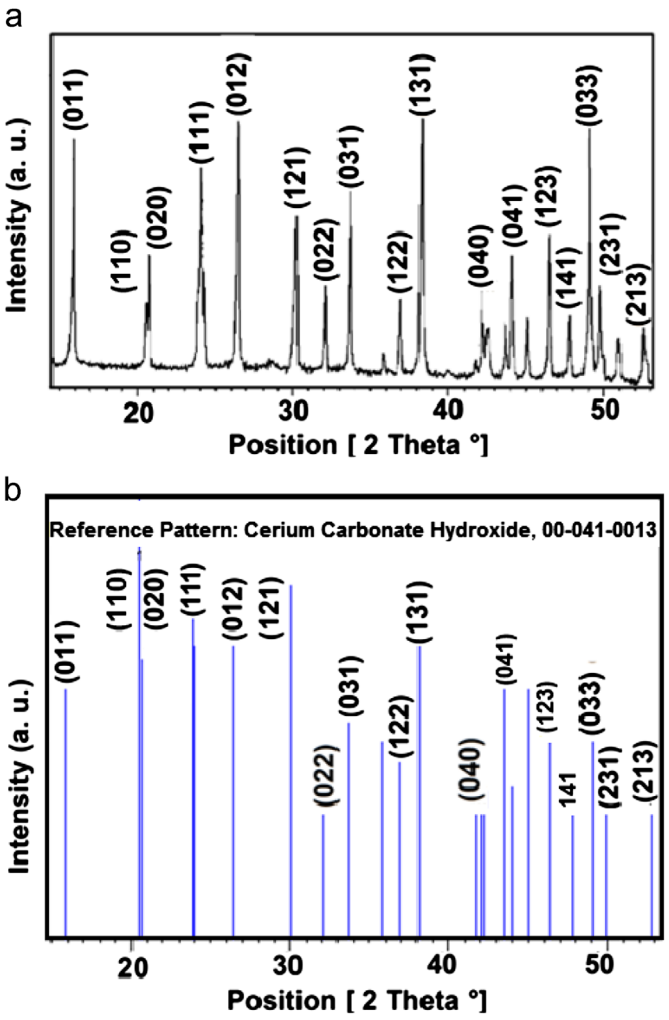

Fig. 1. (a) XRD patterns of $CeCO_3OH$ shuttle microstructures synthesized by the hydrothermal method. (b) XRD patterns of $CeCO_3OH$ bulk materials cerium carbonate hydroxide (Ref. patterns: 00-041-0013).

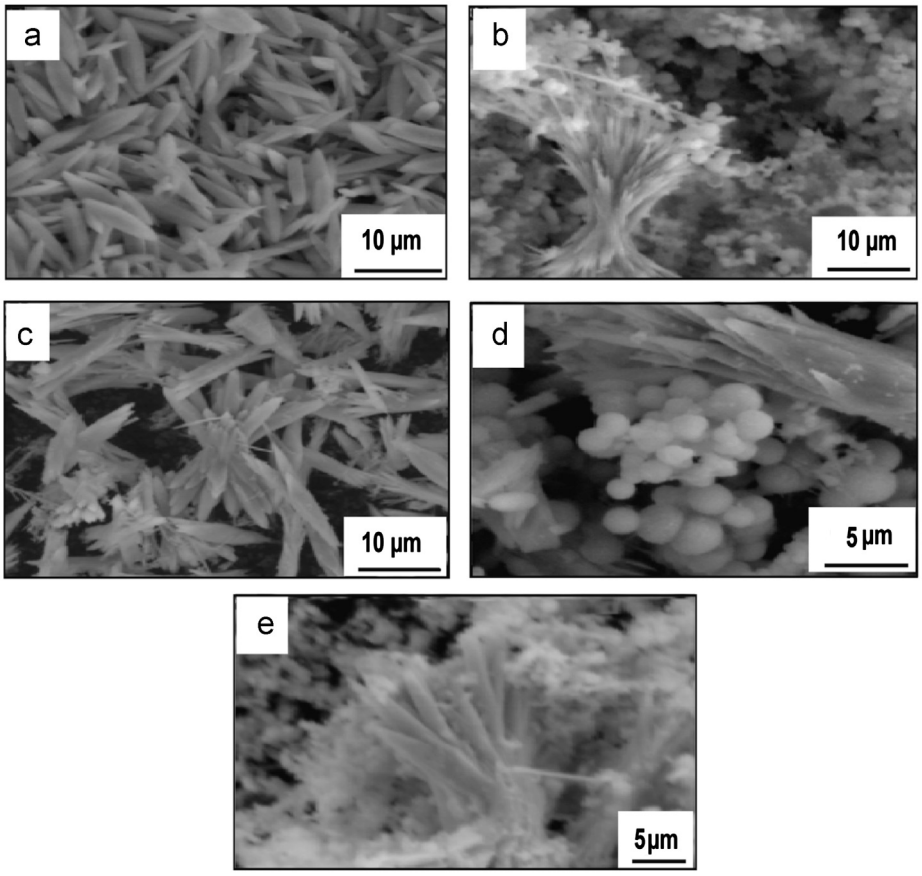

Fig. 2. SEM images for the products prepared with different molar ratios [CTAB/Ce]:(a) 1/1, (b) 1/2 and (c) 2/1 and (d) sample prepared in the absence of CTAB. (e) SEM image of CeO_2 obtained by calcining $CeCO_3OH$ in air at 300 °C for 1 h.

products. Indeed, the $CeCO_3OH$ nonmaterial with shuttle morphology was obtained when the molar ratio CTAB/Ce = 1/1. The diameter of the shuttle materials decreased gradually from about 800 nm (in the central part) to several nanometers (at the ends) and the typical lengths were of several micrometers. In this case, the protective layers formed by the capped CTA^+ on the oxygen surface lead to homogenous and dispersed particles as seen in Fig. 2a. When the molar ratio CTAB/Ce = 1/2, the products were composed of two types of particles with a distinctive morphology: a large amount of spherical particles with some aggregate particles with shuttle morphology as seen in Fig. 2b. When increasing the molar ratio up to 2/1, some $CeCO_3OH$ shuttles were reassembled into bundle-like structures as shown in Fig. 2c. Guo et al. [21] prepared triangular $CeCO_3OH$ microplates, using the same precursors and CTAB as surfactant in hydrothermal conditions at 150 °C for 16 h. The same shuttle morphology with smaller dimensions was obtained for $CeCO_3OH$ prepared in the presence of polyvinyl alcohol (PVA) used as a capping reagent [22].

Thus, we can conclude that the experimental conditions as well as the nature of the surfactant affect the morphology and the size of the final product.

Based on our experimental results, we can assume that CTAB plays a significant part in determining the morphology of the final product. In fact, when the same reaction was carried out without CTAB, agglomerated sheets and spherical particles were obtained (Fig. 2d.). Thus, shuttle morphology is obtained through seed growth in the presence of CTAB molecules. As a surfactant, CTAB is adsorbed selectively by the different planes of the $CeCO_3OH$ seeds promoting lower surface tension which results in a different growth rates of the different planes to form the shuttle structures. The material growth change induced by the adsorbed surfactant molecules is the main factor controlling the final product morphology. The possible mechanism for the $Ce(OH)CO_3$ formation under hydrothermal conditions may be summarized by the following reactions [20]:

$$[Ce(H_2O)_n]^{3+} + H_2O \rightarrow [Ce(OH)(H_2O)_{n-1}]^{2+} + H_3O^+ \quad (1)$$

$$CO(NH_2)_2 + 2H_2O \rightarrow CO_3^{2-} + 2NH_4^+ \quad (2)$$

$$[Ce(OH)(H_2O)_{n-1}]^{2+} + CO_3^{2-} \rightarrow Ce(OH)CO_3 + (n-1)H_2O \quad (3)$$

3.3. Thermal analysis

The thermal study of the as-prepared $CeCO_3OH$ obtained with the molar ratio [CTAB:Ce] = 1:1 was performed in air from room temperature to 700 °C (Fig. 3). The exothermic peak attributed to the combustion of the residual surfactant was observed at around 250 °C. A second thermal event

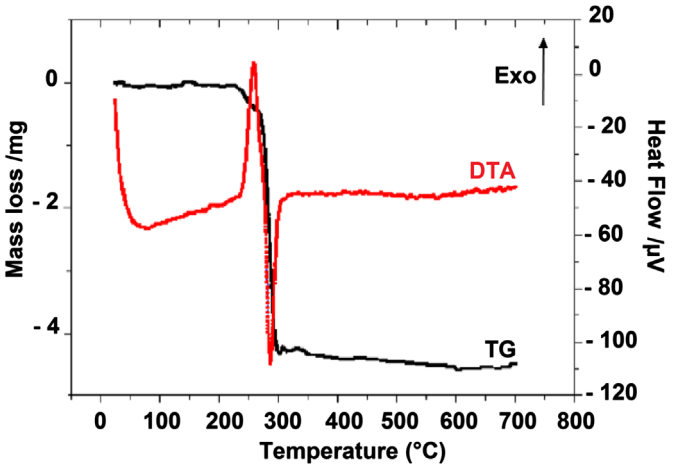

Fig. 3. TG/DTA curves of the as-obtained $CeCO_3OH$ structures.

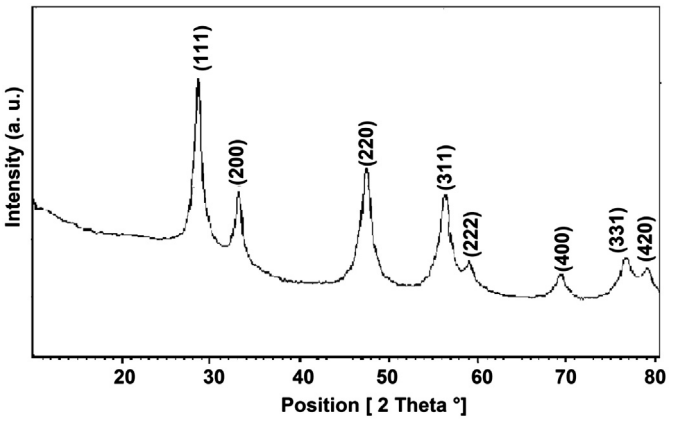

Fig. 4. XRD patterns of CeO_2 nanomaterials.

characterized by an endothermic peak at approximately 280 °C was observed, which corresponds to the thermal decomposition–oxidation process of $Ce(OH)CO_3$ to CeO_2. The corresponding weight loss between 270 and 500 °C is about 21.2%, less than the theoretical value, 24.4% calculated from reaction (4) when $CeCO_3OH$ is fully decomposed at 500 °C.

Fig. 4 shows the XRD patterns for $CeCO_3OH$ after heat treatment at 300 °C for 1 h. All the diffraction peaks for the obtained product can be readily indexed to pure CeO_2 (space group: Fm3m) with lattice constant $a=5.410$ Å (JCPDS No.43-1002). The phase transformation of $CeCO_3OH$ into CeO_2 after the heat treatment can be elucidated by the following equation:

$$4CeOHCO_3+O_2 \rightarrow 4CeO_2+4CO_2+2H_2O \quad (4)$$

Fig. 2e. shows the SEM image of calcined $CeCO_3OH$ materials. The obtained CeO_2 nanomaterials show agglomerated shuttle morphology of approximately the same size and a large number of undefined-shaped particles. In this case, the nanomaterials partially preserve the same morphology during the calcination process at about 300 °C, as their size increases. The crystallite size of calcined $CeCO_3OH$ was found to be 30 nm according to peaks (111) and (2 2 0) using the Debye Scherrer approximation [23], which is defined as ($D=0.9\lambda/(\varepsilon \cos\theta)$), where λ is the wave length of the X-ray ($\lambda=1.5418$ Å), ε is the full width at half maximum (FWHM, radian) and θ is the Bragg angle (degree).

3.4. Electrochemical measurements

The electrochemical activity of the obtained cerium hydroxide carbonate shuttle morphology was studied by measuring the cyclic voltammetry (CV) data. The CV results depicted in Fig. 5a were recorded for the 1st and 20th cycles at room temperature with a scan rate of 50 mV/s in the range [−1 to 1.5 V]. The CV results showed a good stability for the as-prepared nanocrystalline $CeCO_3OH$ shuttle morphology. The curves showed a single oxidation and reduction process. The cathodic current peak was observed at about 0.2 V, which corresponds to the reduction process. The anodic peak current near 0.69 V was assigned to the oxidation process. These two phenomena happens simultaneously with the intercalation/deintercalation of Li^+.

As seen in Fig. 5a, the CV pattern after extended scans of up to 20 cycles registered a perfect overlap of both anodic and cathodic peaks in the respective positions, thereby confirming the excellent cycling reversibility of the as-synthesized materials upon extended cycling. The absence of even a minimal deviation from the anodic/cathodic peak positions upon

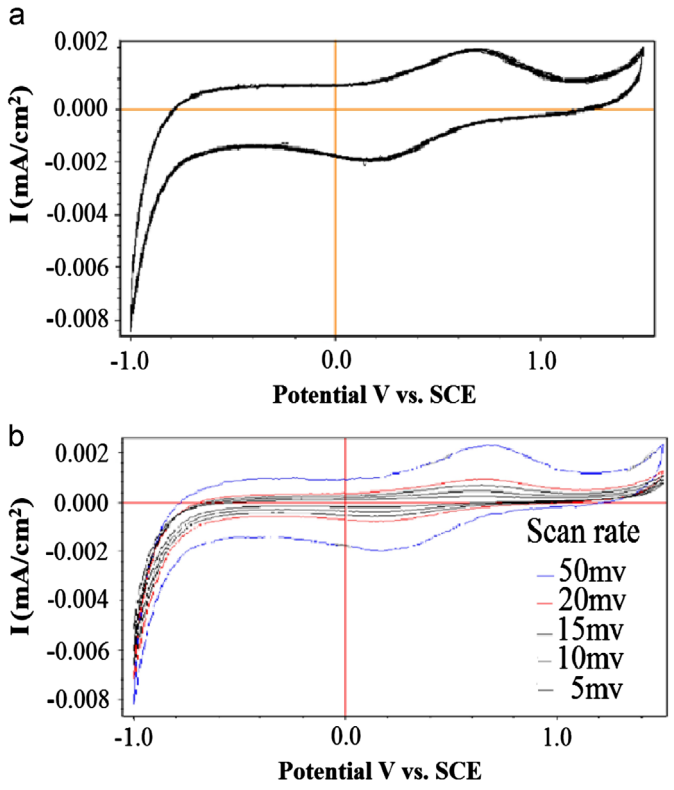

Fig. 5. (a) Cyclic voltammetric reponses of $CeCO_3OH$ recorded at 50 mV/s scan rate from 1st to 20th cycles at room temperature.(b) Cyclic voltammograms of $CeCO_3OH$ compound obtained at different potential scan rates: 5, 10, 15, 20 and 50 mV/s.

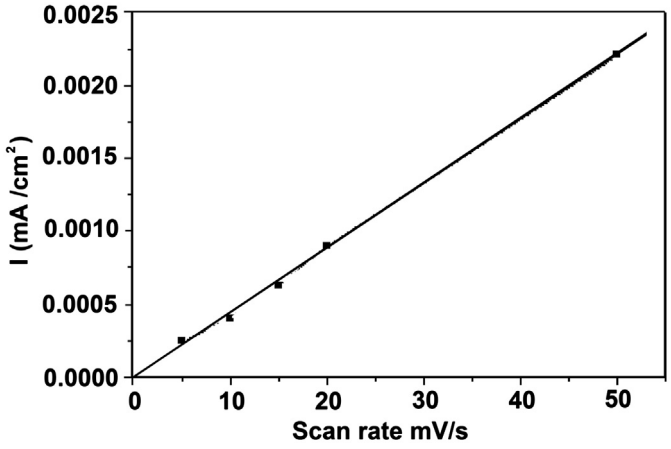

Fig. 6. Voltammetric anodic current (I) versus scan rate for $CeCO_3OH$.

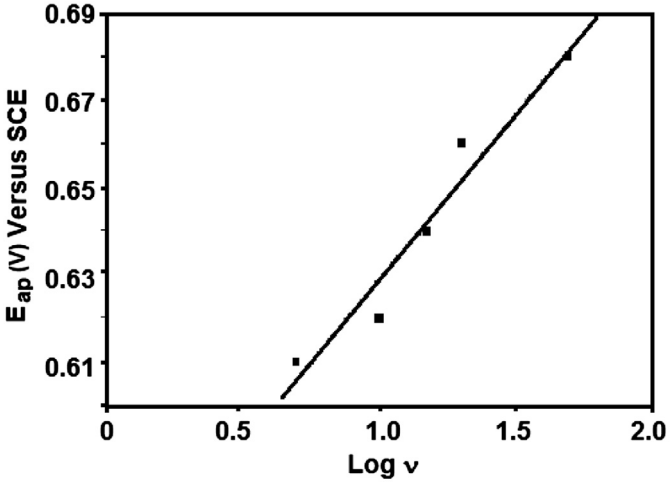

Fig. 7. Anodic peaks potential variation of cyclic voltammograms for the $CeCO_3OH$ electrode as a function of Log υ.

extended cycling confirms the absence of degradation problems which can affect the $CeCO_3OH$ cathode. The voltammograms are almost symmetric, indicating that an excellent electrochemical reversibility was established after the initial cycle. The excellent stability of $CeCO_3OH$ nanocrystallites makes it an interesting possible future electrode for rechargeable lithium cells.

The cyclic voltammograms of the $CeCO_3OH$ compound recorded at different scan rates are shown in Fig. 5b. The anodic current peak increases and its potential shifts slightly in the positive direction with increasing scan rate. This phenomenon indicates the dynamics of the lithium intercalation/deintercalation occurring in the material to provide electroneutrality (Fig. 6).

Fig. 7 shows that the anodic peak potential (E_{ap}) has a linear dependence on Log(υ). In this case, the potential peak can be expressed as in Eq. (5): $E_{ap} = 2.3RT/2\alpha nF$ Log υ [24], where υ is the scan rate, R is the gas constant, T is the electrochemical cell temperature, α is the charge transfer coefficient, n is the number of exchanged electrons and F the Faraday constant. So, this formula allows us to determine the value of the charge transfer coefficient α calculated from the slope in Fig. 7. The calculated value of α is equal to 0.182. Sun et al. [25] assume that when $\alpha < 0.3$, the $CeCO_3OH$ system will tend toward the charging process.

4. Conclusion

$CeCO_3OH$ nanostructures with different morphologies were prepared with the hydrothermal method in the presence of the CTAB surfactant that plays an important role in the growth $CeCO_3OH$ nanomaterials with shuttle morphology. Furthermore, CeO_2 material was obtained after the calcination of $CeCO_3OH$ at 300 °C. The $CeCO_3OH$ material exhibits an excellent electrochemical reversibility, which is important for practical applications such as an electrode material for a lithium ion battery. Therefore, doping with a small amount of rare earth ions (Sm^{3+}, La^{3+}, Pr^{3+}) and controlling the size of the nanocrystallites are two efficient ways of enhancing electrochemical performances such as the energy density and the discharge capacity.

References

[1] G. Zhiyan, D. Fanglin, C. Zuolin, Hydrothermal synthesis of single-crystalline $CeCO_3OH$ flower-like nanostructures and their thermal conversion to CeO_2, Materials Chemistry and Physics 113 (2009) 53–56.
[2] S. Genli, Q. Wang, W. Zhen, C. Yunfa, Hydrothermal synthesis of CeO_2 nano-octahedrons, Materials Letters 65 (2011) 1211–1214.
[3] N. Izu, S. Nishizaki, T. Itoh, W. Shin, I. Matsubara, M. Nishibori, Resistive oxygen sensor using ceria–zirconia sensor material and ceria–yttria temperature compensating materiaal for lean-burn engine, Journal of the Ceramic Society of Japan 115 (2007) 688–691.
[4] E. Bekyarova, P. Fornasiero, J. Kaspar, M. Graziani, CO oxidation on Pd/CeO_2–ZrO_2 catalysts, Catalysis Today 45 (1998) 179–183.
[5] X.Y. Wang, S.R. Wang, S.P. Wang, Y.Q. Zhao, J. Huang, S.M. Zhang, W.P. Huang, S.H. Wu, CuO/$Ce_xSn_{1-x}O_2$ catalysts: synthesis, characterization, and catalytic performance for low-temperature CO oxidation, Catalysis Letters 112 (2006) 115.
[6] X.Q. Fu, C. Wang, H.C. YU, Y.G. Wang, T. Hwang, Fast humidity sensors based on CeO_2 nanowires, Nanotechnology 18 (2007) 145503–145506.
[7] M. Crocker, U.M. Graham, R. Gonzalez, G. Jacobs, E. Morris, A. M. Rubel, R. Andrews, Preparation and characterization of cerium oxide templated from activated carbon, Journal of Materials Science 42 (2007) 3454–3464.
[8] K. Zhou, Z. Yang, S. Yang, Highly reducible CeO_2 nanotubes, Chemistry of Materials 19 (2007) 1215–1217.
[9] A. Vantomme, Z.Y. Yuan, G.H. Du, B.L. Su, Morphology-controllable synthesis of CeO_2 on a Pt electrode, Langmuir 21 (2005) 1132.
[10] H.X. Mai, L.D. Sun, Y.W. Zhang, R. Si, W. Feng, H.P. Zhang, H.C. Liu, C.H. Yan, Shape-selective synthesis and oxygen storage behavior of ceria nanopolyhedra, nanorods and nanocubes, Journal of Physical Chemistry B 109 (2005) 24380–24385.
[11] M.L. Dos Santos, R.C. Lima, C.S. Riccardi, R.L. Tranquilin, P.R. Bueno, J.A. Varela, E. Longo, Preparation and characterization of ceria nanospheres by microwave-hydrothermal method, Materials Letters 62 (2008) 4509.
[12] W. Shurong, Z. Jun, J. Junqing, Li. Rui, Zhu. Baolin, Xu. Mijuan, W. Yan, C. Jianliang, L. Minyan, Y. Zhongyong, Z. Shoumin, H. Weiping, S. Wu, Porous ceria hollow microspheres: synthesis and characterization, Microporous and Mesoporous Materials 123 (2009) 349–353.

[13] R.J. Qi, Y.J. Zhu, G.F. Cheng, Y.H. Huang, Sonochemical synthesis of single-crystalline $CeOHCO_3$ rods and their thermal conversion to CeO_2 rods, Nanotechnology 16 (2005) 2502–2506.
[14] Q. Yuan, H.H. Duan, L.L. Li, L.D. Sun, Y.W. Zhang, C.H. Yan, Controlled synthesis and assembly of ceria-based nanomaterials, Journal of Colloid and Interface Science 335 (2009) 151–167.
[15] H.X. Mai, L.D. Sun, Y.W. Zhang, R. Si, W. Feng, H.P. Zhang, H.C. Liu, C.H. Yan, Shape-selective synthesis and oxygen storage behavior of ceria nanopolyhedra, nanorods, and nanocubes, Journal of Physical Chemistry B 109 (2005) 24380–24385.
[16] S. Chen, S.H. Yu, B. Yu, L. Ren, W. Yao, H. Colfen, Solvent effect on mineral modification: selective synthesis of cerium compounds by a facile solution route, Chemistry European Journal 10 (2004) 3050–3058.
[17] Z.H. Han, N. Guo, K.B. Tang, S.H Yu, H.Q. Zhao, Y.T. Qian, Hydrothermal crystal growth and characterization of cerium hydroxycarbonates, Journal of Crystal Growth 219 (2000) 315–318.
[18] G. Li, S. Feng, L. Li, Structural stability and valence characteristics in cerium hydrothermal systems, Journal of Solid State Chemistry 126 (1996) 74–79.
[19] C.L. Robert, J.W. Long, E.M. Lucas, K.A. Pettigrew, R.M. Stroud, M. S. Doescher, D.R. Rolison, Sol–gel-derived ceria nanoarchitectures: synthesis, characterization, and electrical properties, Chemistry of Materials 18 (2006) 50–58.
[20] F. Zhou, X. Zhao, H. Xu, C. Yuan, CeO_2 spherical crystallites: synthesis, formation mechanism, size control, and electrochemical property study, Journal of Physical Chemistry C 111 (2007) 1651–1657.
[21] Z. Guo, F. Du, G. Li, Z. Cui, Synthesis of single-crystalline $CeCO_3OH$ with shuttle morphology and their thermal conversion to CeO_2, Inorganic Chemistry 45 (2006) 4167–4169.
[22] Z. Guo, F. Du, G. Li, Z. Cui, Synthesis of single-crystalline $CeCO_3OH$ with shuttle morphology and their thermal conversion to CeO_2, Crystal Growth and Design 8 (2008) 2674–2677.
[23] H.P. Klug, L.E. Alexander, X-ray Diffraction Procedures, Wiley-Interscience, New York, 1974.
[24] M. Ben Moussa, M. Abdellaoui, H. Mathlouthi, J. Lamloumib, A. Percheron Guégan, Electrochemical properties of the $MmNi_{3.55}Mn_{0.4}Al_{0.3}CO_{0.4}Fe_{0.35}$ compounds, Journal of Alloys and Compounds 400 (2005) 239–244.
[25] L. Sun, G.X. Wang, H.K. Liu, D.H. Bradhurst, S.X. Dou, Synthesis of nonstoichiometric amorphous Mg-based alloy electrodes by mechanical milling, Electrochemical and Solid-State Letters B 3 (2000) 121–124.